1-1-2017

Minimization of Stack Mass in Miniature PEM Fuel Cell Systems with DC/DC Converters

Yijin Wei
Massachusetts Institute of Technology

Denise A. McKahn
Smith College, dmckahn@smith.edu

Proceedings of the ASME 2017 15th International Conference on Fuel Cell Science, Engineering and Technology
FUELCELL2017
June 26-30, 2017, Charlotte, North Carolina, USA

FUELCELL2017-3713

MINIMIZATION OF STACK MASS IN MINIATURE PEM FUEL CELL SYSTEMS WITH DC/DC CONVERTERS

Yijin Wei*
Massachusetts Institute of Technology
School of Engineering
Cambridge, MA, 02139

Denise A. McKahn
Smith College, Picker Engineering Program
Northampton, MA, 01063
Contact e-mail: dmckahn@smith.edu

ABSTRACT

Polymer electrolyte membrane (PEM) fuel cells have been explored as a clean battery replacement in portable and miniature applications where total system mass and specific energy density (Wh/kg) are critical design constraints. By coupling a boost (step-up) DC/DC converter with a miniature PEM fuel cell stack, the total power system mass can be reduced while providing voltage regulation capabilities not available with a fuel cell alone. This configuration is applied to the design of a controlled meteorological (CMET) balloon power system as a case-study. In this work, we designed and tested three different micro-power DC/DC boost converters that were deployed in series with a PEM fuel cell stack. Testing of the converters revealed a transition region in which the converter output voltage is hysteretic, not well regulated, and dependent on the input voltage. As a result, it is important to identify the minimal stable and reliable input voltage to a given DC/DC converter in order to minimize the fuel cell power system mass. An optimization strategy is presented here that enables the minimization of PEM fuel cell stack mass by identifying the appropriate DC/DC converter input voltage subject to the dimension constraints of the fuel cell components. Prototype DC/DC converters were then experimentally tested in direct connection to a miniature two-cell PEM fuel cell stack.

1 INTRODUCTION

Polymer electrolyte membrane (PEM) fuel cells have been explored recently for lightweight vehicular applications as a clean replacement of batteries, such as the unmanned lightweight vehicles [1] and meteorological balloons [2]. The application of interest in this work is to power the altitude control, data acquisition, data storage and communication system on controlled meteorological (CMET) balloons used for tracing gas species and collecting meteorological data [3]. As with the unmanned aerial system design, the CMET balloon power system must have minimal mass and provide power reliably in a typical flight of 15 hours. The CMET balloons are currently powered by lithium-ion batteries with a specific energy density of approximately 300 Wh/kg. For 10-50 W portable fuel cell power systems, the Department of Energy has targeted specific power densities of 45 W/kg and specific energy densities of 650 Wh/kg [4].

Because fuel cell stack output voltage is variable and dependent upon the current drawn from the stack, there are a variety of electrical system configurations that have been explored for a range of power conditioning needs. Due to the relatively slower fuel cell system time response, compared with batteries, there exists an opportunity to explore the degree of hybridization that is uniquely optimal for each application [5]. Fuel cells are often hybridized with batteries to provide a higher peak power than each individual component with high efficiency and low costs [6]. Without a DC/DC converter, the fuel cell and battery hybrid power system voltage is constrained and regulated by the batteries [7] whose state of charge must be well regulated. This is a common power system configuration in medium to high power

*Previously affiliated with Smith College.

applications, such as vehicular transport.

Several electrical configuration have been proposed for hybrid fuel cell power systems [8]. A load-leveling or load-sharing hybrid configuration supplements the fuel cell current with battery current. A load following fuel cell can be connected directly to the load with bi-directional DC/DC converter and battery. However, most power conditioning is focused on high power applications where mass is not a critical design constraint.

Additionally, one must consider the length of time needed to store energy and from where the primary energy sources are being harnessed. For example, fuel cells have been used with photovoltaic panels for operations at night [9,10] and to generate reliable electricity in rural areas [11].

In low power applications that require a well regulated output voltage from the power supply, the fuel cell stack voltage should be regulated. A voltage regulator steps down and regulates a constant output voltage. However, the fuel cell stack connected with the voltage regulator should have more cells to produce a higher input voltage to the voltage regulator, which increases the system mass. Boost DC/DC converters can be used to step up the input voltage. A boost DC/DC converter is an electronic device that produces a regulated DC output voltage from an unregulated DC input voltage of lower magnitude and higher current. The fuel cell stack connected with a boost DC/DC converter draws current from the fuel cell. Therefore, the fuel cell active area increases and the number of cells needed in the stack decreases. Indeed, a larger active area increases the mass of each component, but this increase is potentially less significant than the mass reduction achieved by using fewer cells in the stack. Therefore, regulating the fuel cell output voltage with a boost DC/DC converter could result in a power system of lower mass.

In higher power applications, a DC/DC converter has been used between lithium-ion batteries and fuel cells [12]. However, their work focused primarily on aligning component voltages. While sparse literature is dedicated to power conditioning in miniature fuel cells, the authors are not aware of optimization strategies that specifically target reduced power system mass.

In this work, we first characterize the static response of DC/DC Boost Converters. We then present an optimization strategy to minimize fuel cell power system mass for a CMET application. The reduction in the overall system mass is critical in order to compete with existing battery technologies. Finally, we test a multi-cell PEM fuel cell stack electrically connected to a DC/DC boost converter and load as a proof-of-concept that can be deployed on a controlled meteorological balloon.

2 DC/DC CONVERTER TESTING

This section details the selection rationale for the specific DC/DC converter package used in this work, the design and assembly of the printed circuit board, and the static performance characteristics of the DC/DC boost converter.

2.1 DC/DC Converter Selection and PCB Design

In our experiments, LTC 3539 manufactured by Linear Technology was chosen as the boost DC/DC converter between the fuel cell stack and load. This converter has a variable output voltage range (1.5-5.25 V) that satisfies the needs for our application. Among the various off-the-shelf micro-power DC/DC converters, LTC 3539 requires the least number of external components, which is beneficial for reducing total system mass. Table 1 shows relevant electric specifications for this DC/DC converter package. Of greatest importance are the minimum input voltage after start-up, V_{in}, the minimum input voltage during startup, and the range of regulated output voltages that can be achieved.

TABLE 1. The critical electric specifications of the LTC 3539 DC/DC boost converter

Minimum V_{in}	Minimum start-up V_{in}	V_{out} range
0.5	0.77 – 0.8 V	1.5 – 5.25 V

This DC/DC converter is offered in an 8-lead 2 mm x 3 mm x 0.75 mm plastic dual-flat no-leads (DFN) package. The chip is connected to five external components (C_1, C_2, L, R_1 and R_2) on a printed circuit board (PCB), as illustrated in Figure 1. The manufacturer recommends adding a 3.3 pF capacitor in parallel with the output capacitor to improve the transient response. This capacitor is not included in our design to minimize the board size and the system mass. The transient response was evaluated under stable input voltages and found to be satisfactory.

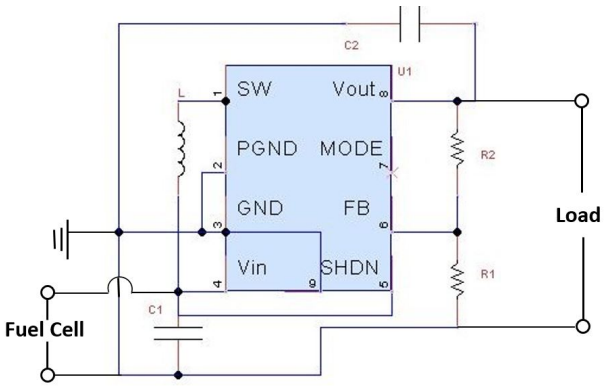

FIGURE 1. Circuit configuration of LTC 3539 with all the external components. In this image, the power source is labeled as a fuel cell.

Three different PCB designs were considered in this work with different voltage output regulation capabilities (1.8 V, 3.3 V and 5 V). These PCBs were printed and assembled by Biettele

Electronics. For each PCB, different external component sizes were selected as described below. These three output voltage levels were specifically selected to power the instrumentation on board the CMET balloon using the three existing voltage buses.

The C_1 capacitor is located at the power input to the electrical system. This capacitor filters fluctuations in the fuel cell output voltage. The manufacturer recommended $C_1 \geq 2.2\,\mu$F, which was deployed throughout this work. Similarly, the output capacitor C_2 stabilizes the converter output voltage. The manufacturer recommended that a $C_2 = 22\,\mu$F to $47\,\mu$F for output voltages of 3 V or greater and C_2 up to $100\,\mu$F is required at lower output voltages. Thus, the 5 V and 3.3 V converter circuits adopt $C_2 = 47\,\mu$F and the 1.8 V converter circuit uses $C_2 = 100\,\mu$F.

For the inductor, L, the manufacturer suggested values between 3.3-4.7 μH and noted that applications where $V_{in} < 1.6$ V should use a $2.2\,\mu$H inductor. Additionally, larger values of inductance will allow greater output current capability. Since the 5 V converter expects a high output current (0.5 A), its inductor is chosen to be $6.8\,\mu$H. The input voltage of the 1.8 V boost converter is generally less than 1.6 V, so a $2.2\,\mu$H inductor was deployed. The 3.3 V converter has a $3.3\,\mu$H inductor.

The values of two resistors R_1, R_2 are related by

$$V_{out} = 1.2\,(1 + \frac{R_2}{R_1}), \tag{1}$$

and are used to obtain the desired output voltage. Using the manufacturer recommended $R_2 = 1$ MΩ to reduce the number of components that differ for each board, we then calculated the required R_1. For output voltages of 5 V, 3.3 V and 1.8 V, R_1 is determined to be 312 kΩ, 571 kΩ and 2 MΩ. Table 2 summarizes the values of all external components for each of the three PCBs.

TABLE 2. External component values for each of the three PCBs. Each PCB was designed to regulate a different output voltage level.

V_{Load}	C_1 (μF)	C_2 (μF)	L (μH)	R_1 (Ω)	R_2 (Ω)
5 V	2.2	47	6.8	312k	1M
3.3 V	2.2	47	3.3	571k	1M
1.8 V	2.2	100	2.2	2M	1M

The same PCB design is deployed for all three prototypes of the DC/DC converter. An assembled PCB will be referred as a DC/DC Integrated Circuit Board (ICB), shown in Figure 2. Table 3 summarizes the mass and size of each prototype.

2.2 ICB Performance

Each DC/DC ICB was bench tested in stand-alone operation prior to being connected with a fuel cell stack. The input voltage to the ICB was provided by an Agilent E3631A power source. A variable resistive load was connected to the output to simulate an electrical load. The input current, input voltage and output voltage were measured. The output current was calculated at steady state with Ohm's Law from the measured output voltage and load resistance. The electrical configuration for the DC/DC ICB static testing is shown in Figure 3. Each DC/DC ICB was tested with a variety of load resistances and input voltages. To minimize power system mass, we must identify the minimal DC/DC ICB input voltage (fuel cell output voltage) required for stable operation under all loading conditions.

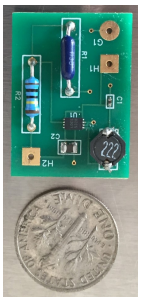

FIGURE 2. The prototype integrated circuit board compared in size to a U.S. dime.

TABLE 3. Mass and size of the three prototypes.

V_{load}	Mass (g)	Size (cm$\times$cm)
5 V	2.5	1.93×2.90
3.3 V	2.7	2.17×2.97
1.8 V	2.6	2.17×2.97

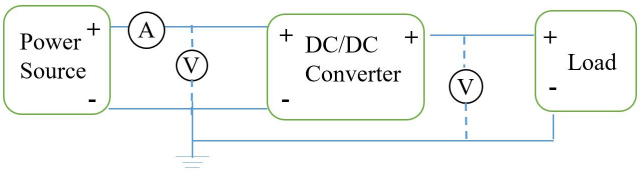

FIGURE 3. Experimental electrical configuration of DC/DC boost converter connected to a power source and a load.

For the 5 V DC/DC ICB, tests were conducted at a sequence of static load resistances from 10-250 Ω. The input and output voltage at each load resistance are plotted in Figure 4.

Each curve in Figure 4 for resistances above 14.8 Ω shows two regions of operation after turn-on: the transition region and the region of normal operation. The minimum input voltage that leads to a positive output voltage is called the turn-on voltage. For input voltages less than the turn-on voltage, a zero output

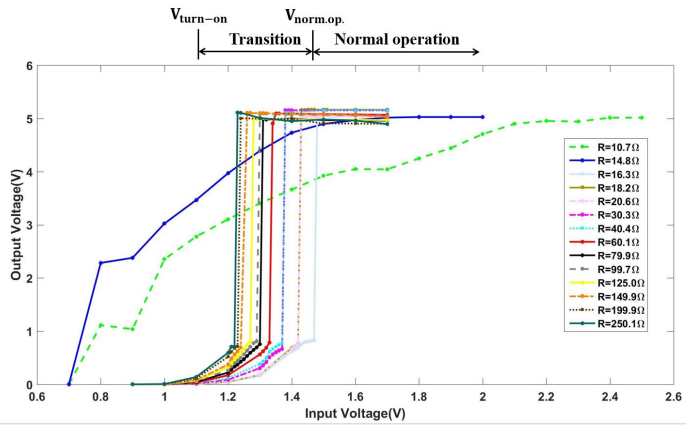

FIGURE 4. Output voltage as a function of input voltage at various load resistances for the 5 V DC/DC ICB.

voltage is observed. The minimum input voltage that leads to the desired regulated voltage is called the normal operation voltage. Input voltages between the turn-on and normal operating voltage are termed transition voltages. The transition region defines the space between turn-on and normal operation.

For the 5 V DC/DC ICB, the turn-on voltage is clearly variable and dependent upon the load resistance. Moreover, the turn-on voltage at resistances above 14.8 Ω is higher than what the data sheet claims (0.88 V). In the normal operation region, the output voltage is well-regulated and centered on 5 V. As load resistance decreases from 250 Ω to 16.3 Ω, the required input voltage for normal operation increases as plotted in Figure 5. For optimization purposes, the experimentally identified relationship between the minimal input voltage required for normal operation and load resistance will be modeled as described in Section 3.

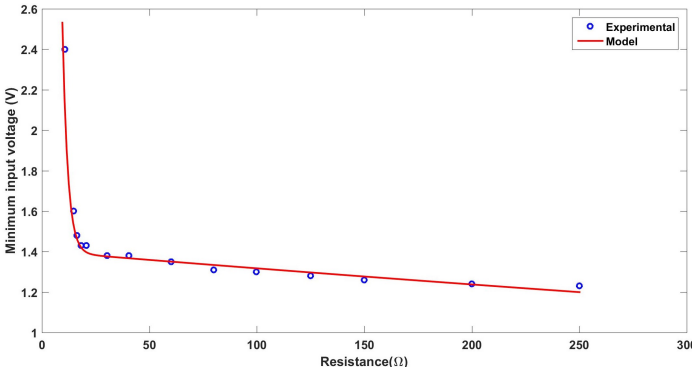

FIGURE 5. Minimum input voltage as a function load resistance for the 5 V ICB.

The turn-on region for load resistances of 10.7 Ω and 14.8 Ω has a much larger range of input voltage before the converter reaches the normal operation. At 10.7 Ω, the converter could not regulate voltage with an input voltage less than 2.1 V. It is possible that at lower resistances, the inductor is completely discharged before the end of an operating cycle, that is, the current through the inductor falls to zero during part of the period. Therefore, the output voltage gain has a response that is different than the converter is designed.

To examine the expected variability in the output voltage at a given load resistance, the 5 V ICB was tested with fixed resistive loads of 151.0 Ω and 15.5 Ω. The experiment was repeated five times as shown in Figure 6 and 7. The converter performance at a load resistance of 151.0 Ω is reproducible with low variability in the output voltage. The performance of the converter shows more variability at the lower load resistance. Note that at 15.5 Ω, an input voltage greater than 1.8 V leads to normal operation in all five trials. The result from the reproducibility test matches the observation from Figure 4 that the output voltage has a different response at the load resistance below 16 Ω.

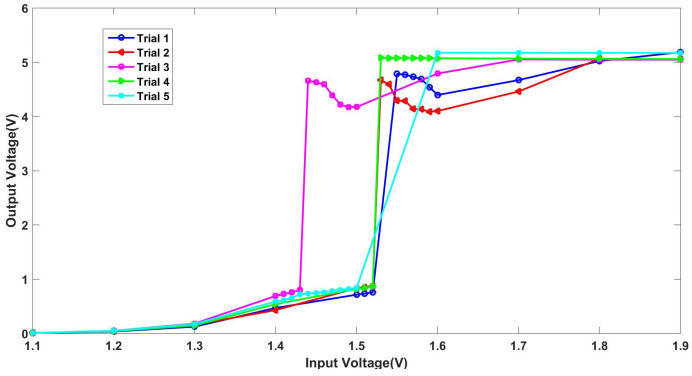

FIGURE 6. ICB output voltage as a function of input voltage at a load resistance of 15.5 Ω in five trials for the 5 V ICB.

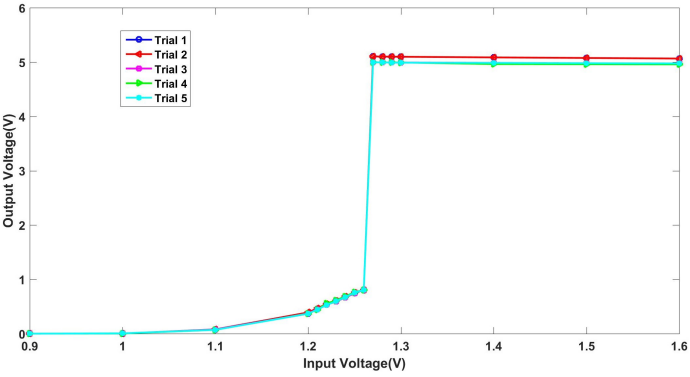

FIGURE 7. ICB output voltage as a function of input voltage at a load resistance of 151.0 Ω in five trials for the 5 V ICB.

These same trends are observed in the 3.3 V ICB as well as the 1.8 V ICB, shown in Figures 8 and 9. Generally, the smaller

the difference between the regulated output voltage and the supplied input voltage, the narrower the transition region and the more closely the minimal input voltage listed in the specification sheet matches the experimentally identified minimal input voltage for normal operation with this DC/DC converter package.

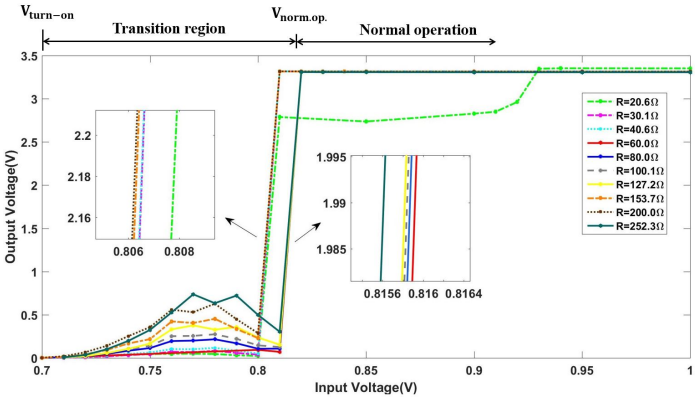

FIGURE 8. Output voltage as a function of input voltage at various load resistances for the 3.3 V converter.

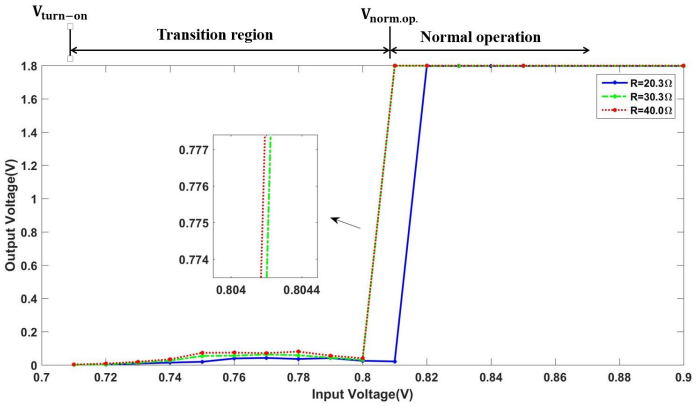

FIGURE 9. Output voltage as a function of input voltage at various load resistances for the 1.8 V converter.

3 OPTIMIZATION STRATEGY

The relationship between the minimal input voltage for normal operation and the load resistance can be combined with the fuel cell polarization characteristics in order to appropriately size the fuel cell stack for minimal system mass. Such reductions in mass are critical to increase the specific power and energy densities of the fuel cell power system and make fuel cells competitive with existing battery technologies. We present a general optimization procedure for sizing the fuel cell stack connected with multiple electric buses each of which is conditioned by a DC/DC ICB. This method is applied to the CMET balloon power system as a case study in Section 4.

3.1 Calculation of Stack Mass

The fuel cell has a physical constraint when the active area is varied, namely, the distance d between the edge of the fuel cell and the edge of the active area is constant. This area is required for sealing and species distribution as well as tie-rods that hold the materials together. As the active area varies, the dimensions of the other fuel cell components also change, shown in Figure 10. The mass of the endplate, endplate gasket and bipolar plate can be calculated with Equation 2. The mass of the gas diffusion later (GDL) and GDL gasket are calculated with Equations 3 and 4 respectively.

$$m = (\sqrt{A} + 2d)^2 t\rho \tag{2}$$

$$m_{\mathrm{GDL}} = At\rho \tag{3}$$

$$m_{\mathrm{GDLg}} = m_{\mathrm{eg}} - At\rho \tag{4}$$

where A is active area, d is distance between the component outer edge and the edge of the active area, t is component thickness, m is component mass and ρ is material density. The miniature PEM fuel cell and stack design used in this work is detailed in [13]. A

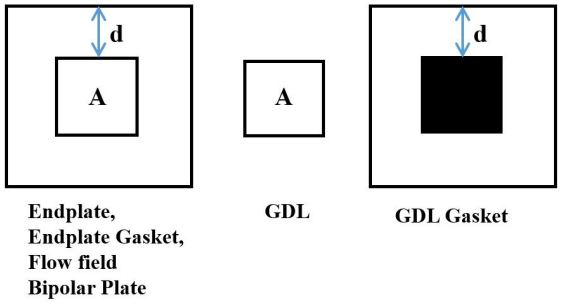

FIGURE 10. Cross section of each fuel cell component (A stands for active area).

fuel cell stack of n cells is comprised of 2 endplates, 2 endplate gaskets, 2 flowfields, $2n$ GDL, $2n$ GDL gaskets, $n-1$ bipolar plates, tie-rods and gas fittings. The mass of the plastic tie-rods and fittings deployed in [13] is assumed to be negligible with respect to the mass of each additional cell within the stack. The mass of the fuel cell stack with n cells is

$$\begin{aligned} m_{stack} =& 2(m_{ep} + m_{ff} + m_{eg}) + 2n(m_{GDL} + m_{GDLg}) \\ &+ (n-1)m_{bp} + m_{tierod} + m_{fitting}. \end{aligned} \tag{5}$$

By Equations 2, 3, 4 and 5, the fuel cell system mass is a function of the number of cells n and the active area A.

3.2 Calculation of Input Voltage and Input Current

When multiple electric buses are connected to a fuel cell stack, the minimum fuel cell stack output voltage is constrained by the DC/DC ICB that requires the greatest minimal input volt-

age for normal operation. As the stand-alone ICB testing shows, the converter output voltage will remain well regulated at the desired level once the input voltage exceeds a threshold. The converter input current is a function of load resistance and input voltage and it can be modeled as shown in Figure 5.

3.3 Decision Variables and Parameters

The number of cells, n, and the active area, A, are to be decided in some optimal fashion in order to minimize the stack mass, which is the objective function. These variables are called decision variables. Since the m electric buses are connected in parallel, the input voltage and input current of each ICB ($V_{\text{in},1}$, $V_{\text{in},2}$, $V_{\text{in},3} \cdots V_{\text{in,m}}$, and $I_{\text{in},1}$, $I_{\text{in},2}$ $I_{\text{in},3} \cdots I_{\text{in,m}}$) are related to fuel cell output voltage $V_{\text{out,fc}}$ and fuel cell output current $I_{\text{out,fc}}$ by Equations 6 and 7.

$$V_{\text{out,fc}} = V_{\text{in},1} = V_{\text{in},2} = V_{\text{in},3} = \cdots = V_{\text{in,m}} \quad (6)$$

$$I_{\text{out,fc}} = I_{\text{in},1} + I_{\text{in},2} + I_{\text{in},3} + \cdots + I_{\text{in,m}} \quad (7)$$

Furthermore, the output voltage per cell, $V_{\text{out,cell}}$, and fuel cell current density, i, are related to the fuel cell output voltage and output current by Equations 8, 9, 10. Equation 9 represents the fuel cell polarization curve that must be established from experimental data. Table 4 shows a summary of the nomenclature used in the optimization process.

$$V_{\text{out,fc}} = n V_{\text{out,cell}} \quad (8)$$

$$V_{\text{out,cell}} = f(i) \quad (9)$$

$$I_{\text{out,fc}} = A\, i \quad (10)$$

The output voltage and output current of the ICBs have been determined by the electric needs of the load, so they are parameters in the optimization. Parameters also include the thickness of the fuel cell components, densities of component materials and the distance between the edge of the active area and the edge of the fuel cell. They are related to the fuel cell component mass by Equation 2−4. Finally, because the ICB behavior is a function of the load resistance, the load resistance of each bus is a parameter.

3.4 CMET Case Study

The optimization procedure is followed to size the fuel cell stack for the CMET power system. We consider the three electric buses ranging from 1.8-5 V during a flight of 15 hours. Figure 11 shows the CMET balloon power system with DC/DC converters deployed as ICBs.

First, the polarization curve of a two-cell PEMFC stack was measured using a cell and stack design as well as materials described in [13]. For optimization purposes, a basis function that adequately captures the activation and ohmic overvoltages at the

TABLE 4. Variables used in the fuel cell mass optimization process

Variable	Symbol
Output voltage of FC stack	$V_{\text{out,fc}}$
Output voltage per cell	$V_{\text{out,cell}}$
Output current of fuel cell	$I_{\text{out,fc}}$
Input current of converters	$I_{\text{in},1}, I_{\text{in},2}, \cdots, I_{\text{in,m}}$
Input voltage of converters	$V_{\text{in},1}, V_{\text{in},2}, \cdots, V_{\text{in,m}}$
Number of cells	n
Active area	A
Fuel cell current density	i
Mass of fuel cell components	m_{ep}, m_{ff}, m_{eg}
	m_{GDL}, m_{GDLg}, m_{bp}

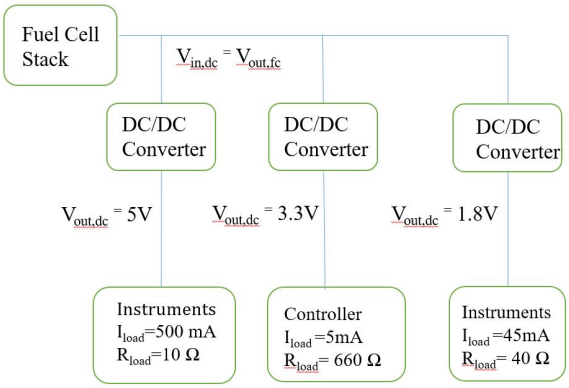

FIGURE 11. CMET balloons power system with DC/DC converters used on ICBs.

expected operating conditions was selected from [14],

$$V_{out,cell} = a_1 + a_2\, i + a_3 \log(i) + a_4 / \exp(0.07i), \quad (11)$$

where $V_{out,cell}$ is the output voltage per cell (V/cell) and i is the stack current density (mA/cm^2). By minimizing the sum of the squared residuals between the measured and estimate cell voltage, the identified model coefficients with 95% confidence bounds are a_1 = 1.928, a_2 = - 0.00743, a_3 = -0.0641, and a_4 =- 0.0699.

Then, the minimum input voltage of the 5 V converter as a function of resistance is fitted with Equation 12. We consider the general case that the ICB was not bench tested at the operating load resistance in the power system. At the equivalent resistance of the 5 V bus (10 Ω), Equation 12 predicts $V_{\text{in,min}} = 2.32$ V

$$V_{\text{in,min}}(R) = 51.69e^{-0.4013R} + 1.402e^{-0.0006235R} \quad (12)$$

Now, we fit the converter input current. We observed that the input current of the DC/DC converter is a function of the input voltage and resistance during normal operation. The 1.8 V converter was bench tested at the load resistance of the 1.8 V electric bus (40 Ω). For 1.8 V converter at 40 Ω, the input current vs. input voltage curve after turn-on was fitted by Equation 13 to minimize the R^2 value.

$$I_{\text{in,1.8V}} = 0.08372e^{V_{\text{in,1.8V}}} + 10^{-6}e^{2.332V_{\text{in,1.8V}}} \quad (13)$$

The load resistance of the 3.3 V converter (660 Ω) was not included in the bench testing. We assume that at 660 Ω, the input current does not change with input voltage. The input voltage must be greater than 1.2 V since the 5 V converter has a turn-on voltage of 1.2 V at high resistances. Thus, the input currents for each resistance at input voltages $\geq$ 1.2 V were averaged and fitted by Equation 14.

$$I_{\text{in,3.3V}}(R) = 0.2775e^{-0.02748R} + 0.07664e^{-0.003935R} \quad (14)$$

Table 5 shows a summary of parameter values in the optimization process.

TABLE 5. Parameter values used in the fuel cell optimization process

Parameter	Value
Thickness of gasket	0.0127 cm
Thickness of bipolar plate	0.1778 cm
Thickness of flow field	0.1143 cm
Thickness of endplate	0.635 cm
Thickness of GDL	0.0381 cm
Density of acrylic (endplate)	1.18 g/cm^2
Density of Buna-N (gasket)	1.25 g/cm^2
Density of graphite bipolar plates/flow fields	2.26 g/cm^2
Density of GDL	0.541 g/cm^2
Distance between the edge of the active area and the edge of fuel cell (d)	1.32 cm
Mass of tie-rods and fittings	2.0 g

For the CMET power system, the optimization problem is infeasible using a stack with less than or equal to 3 cells because the resultant fuel cell operating voltage is not great enough as an input to the ICB for stable operation. The fuel cell system mass was therefore optimized for cases where the integer number of cells is varied from 4-10. For each number of cells, the required active area is determined, from which the fuel cell stack mass can be calculated. The resulting power system mass as a function of the number of cells is convex with a minimum at six cells. The resultant configuration is presented in Table 6. Note that the mass of this six-cell stack does not include the mass of hydrogen and subsystems.

TABLE 6. The optimal fuel cell stack when $R_{\text{load}} = 10\,\Omega$ using DC/DC ICBs.

# cells	Stack mass	Active area	Current density	$V_{\text{out,fc}}$
6	234.7 g	22.5 cm^2	83.4 mA/cm^2	3.07 V

The total system mass was calculated for the stack using DC/DC converters and load resistance of 250 Ω for the 5 V bus, resulting in a fuel cell stack mass of 72.5 g and a total power system mass of 95.3 g. The specific energy density 193 Wh/kg and specific power density is 13 W/kg. We are making progress towards the Department of Energy's 2020 target for fuel cell specific power density in portable power applications (45 mW/g) and the specific energy density of off-the-shelf lithium-ion batteries (approximately 300 Wh/kg) [4].

4 FUEL CELL STACK AND DC/DC ICB

The three prototype DC/DC ICBs used for the three electric buses of the CMET onboard system were tested by directly connecting each of them to a 2-cell fuel cell stack. Because the 5 V ICB exhibited the widest range in the transition region and the greatest variability in expected output voltage at low load resistance, we show the experimental results from that 5 V test here.

The chosen MEA is a Nafion 212 membrane with an active area of 4.84 cm^2, and a catalyst layer of 0.3 mg/cm^2 Pt/C on the anode and cathode. Straight channels are used on both anode and cathode flow fields using a single graphite bipolar plate. The anode and cathode channel depths and widths are 0.032 inches. The gas diffusion layer is a single sided ETeK ELAT.

The fuel cell membrane was assembled dry and the sealing of the fuel cell was checked to prevent gas leakages. Dry industrial grade hydrogen was pressure regulated to 1.8 psig at the anode, and a stream of dry air was delivered to the cathode at a fixed mass flow rate of 200 standard cubic meter/minute (sccm). The cathode exhaust was vented directly to the room. The anode was operated in dead-ended mode with no flow leaving the anode exhaust manifold. To minimize system mass, neither the cathode or anode supply gases are humidified.

Figure 12 plots the output voltage of the fuel cell stack, the output voltage of the 5 V ICB and the current through the load as a function of time. When the load current was increased at 0.01 A increments during the 1-3 min time period, the fuel cell

stack output voltage dropped gradually from 1.59 V to 1.08 V as expected. The converter output voltage remained regulated at 5±0.06 V from 1-2.5 min. We were able to increase the current to 0.12 A before the low load resistance caused the DC/DC ICB to stop functioning. Then, at 3.1 min, the load current was decreased slightly to a level where the converter was able to regulate the voltage before. However, the converter could no longer regulate voltage at 5 V, indicating hysteresis in the ICB minimum input voltage. From 5-7 min, the load current simulated onboard instruments turning on and off and the DC/DC ICB satisfactorily regulated the output voltage at 5 V.

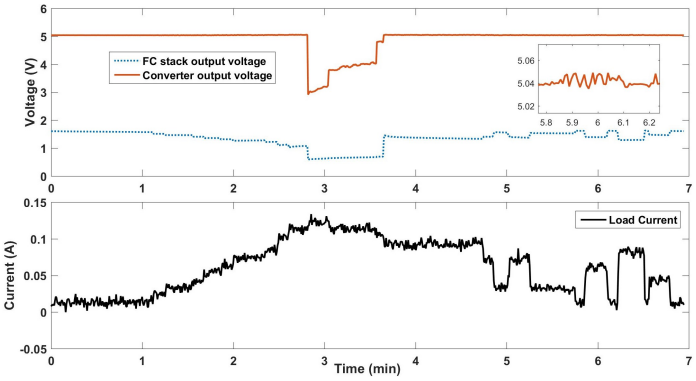

FIGURE 12. Responses of fuel cell stack and the 5 V DC/DC ICB.

5 CONCLUSION

DC/DC ICBs can be designed to be directly coupled with PEMFC stacks for voltage output regulation and step-up DC/DC voltage output capabilities. The static testing of these ICBs showed that the voltage at which the DC/DC converter reaches normal operation depends on the input voltage and load resistance. Moreover, the range of input voltage within the transition region is a function of the DC/DC converter output voltage. The larger the output voltage, the larger the transition region. For one converter prototype, the turn-on voltage when deployed across a wide range of resistances is higher than the data sheet specifies. As a result, a detailed static map is required of the DC/DC circuit in order to characterize performance and adequately design the desired input voltage and resultant PEMFC stack size. An optimization method is developed for the configuration that couples DC/DC converters with a fuel cell stack. Significant progress has been made toward achieving a competitive specific energy and power density when compared to lithium-ion batteries.

REFERENCES

[1] Gadalla, M., and Zafar, S., 2016. "Analysis of a hydrogen fuel cell-pv power system for small uav". *International Journal of Hydrogen Energy,* ***41***.

[2] McKahn, D., and Zhao, X., 2012. "Channel dimensions constraints for miniature low humidity pem fuel cells". *Proceedings of 2012 ASME Fuel Cell Science and Technology Conference, ESFuelCell2012-91504*.

[3] Apel, E., and et al, 2010. "Chemical evolution of volatile organic compounds in the outflow of the mexico city metropolitan area". *Atmos. Chem. Phys.,* ***10***, pp. 2353–2375.

[4] Spendelow, J., Ho, D., and Papageorgopoulos, D., May 2011. Revised portable power fuel cell targets. Tech. rep., Department of Energy.

[5] Suh, K.-W., and Stefanopoulou, A. G., 2005. "Coordination of converter and fuel cell controllers". *International Journal of Energy Research,* ***29***(12), pp. 1167–1189.

[6] Jiang, Z., and Dougal, R. A., 2006. "A compact digitally controlled fuel cell/battery hybrid power source". *IEEE Transactions on Industrial Electronics,* ***53***(4), June, pp. 1094–1104.

[7] A. Nishizawa, J. Kallo, O. G. J. W.-U., 2013. "Fuel cell and li-ion battery direct hybridization system for aircraft applications". *Journal of Power Sources,* ***222***, pp. 294–300.

[8] Stefanopoulou, A. G., and Suh, K.-W., 2007. "Mechatronics in fuel cell systems". *Control Engineering Practice,* ***15***(3), pp. 277 – 289.

[9] Cestino, E., 2006. "Design of solar high altitude long endurance aircraft for multi payload and operations". *Aerospace Science and Technology,* ***10***.

[10] Davat, B., and et al. "Fuel cell-based hybrid systems". *Advanced Electromechanical Motion Systems & Electric Drives Joint Symposium*, p. 111.

[11] Rekioua, D., Bensmail, S., and Bettar, N., 2014. "Development of hybrid photovoltaic-fuel cell system for standalone application". *International Journal of Hydrogen Energy,* ***39***(3), pp. 1604 – 1611.

[12] Verstraete, D., Lehmkuehler, K., Gong, A., Harvey, J., Brian, G., and Palmer, J., 2014. "Characterisation of a hybrid, fuel-cell-based propulsion system for small unmanned aircraft". *Journal of Power Sources,* ***250***, pp. 204–211.

[13] McKahn, D., 2015. "Influence of gas channel depth in self-humidified miniature pem fuel cells with dead-ended anode". *International Journal of Hydrogen Energy,* ***40***, p. 71687181.

[14] Schilter, A., McKay, D., and Stefanopoulou, A., 2006. "Parameterization of fuel cell stack voltage: Issues on sensitivity, cell-to-cell variation, and transient response". *Proceedings of the ASME 4th International Conference on Fuel Cell Science, Engineering and Technology,* ***FUELCELL2006-97177***.